Acta Crystallographica Section B
Structural Science
ISSN 0108-7681

The incommensurately and commensurately modulated crystal structures of chromium(II) diphosphate

Lukáš Palatinus,[a]*‡ Michal Dušek,[a] Robert Glaum[b] and Brahim El Bali[c]

[a]Institute of Physics, Academy of Sciences of the Czech Republic, Na Slovance 2, 182 21 Prague, Czechia, [b]Department of Inorganic Chemistry, University of Bonn, Gerhard-Domagk-Strasse 1, D-53121 Bonn, Germany, and [c]Laboratory of Mineral Solid Chemistry, Department of Chemistry, Faculty of Sciences, PO Box 624, 60000 Oujda, Morocco

‡ Present address: Ecole Polytechnique Fédérale de Lausanne, Laboratoire de Cristallographie, BSP, CH-1015 Lausanne, Switzerland.

Correspondence e-mail: palat@fzu.cz

Received 5 January 2006
Accepted 20 March 2006

Chromium(II) diphosphate, $Cr_2P_2O_7$, has an incommensurately modulated structure at ambient conditions with a = 7.05, b = 8.41, c = 4.63 Å, β = 108.71° and $\mathbf{q}$ = (−0.361, 0, 0.471). It undergoes a phase transition towards a commensurate structure with a commensurate $\mathbf{q}$ vector, $\mathbf{q} = (-\frac{1}{3}, 0, \frac{1}{2})$, at T_c = 285 K. The incommensurate structure has been solved by the charge-flipping method, which yielded both the basic positions of the atoms and the shapes of their modulation functions. The structure model for the commensurate structure was derived directly from the incommensurate structure. The structure analysis shows that the modulation leads to a change of the coordination of the Cr^{2+} ions from distorted octahedra in the average structure towards a sixfold coordination in the form of a more regular octahedron and a fivefold coordination in the form of a square pyramid. The fivefold and sixfold coordination polyhedra alternate along the lattice direction **a** with the pattern 5-6-5 5-6-5 in the commensurate structure. In the incommensurate structure this pattern is occasionally disturbed by a 5-6-5-5 motif. Both structures can be described in superspace using the same superspace group and a similar modulated structure model. The same superspace model can also be used for the low-temperature phases of other metal diphosphates with the thortveitite stucture type at high temperature. Their low-temperature structures can be obtained from the superspace model by varying the $\mathbf{q}$ vector and the origin in the internal dimension t_0.

1. Introduction

Diphosphates $M_2P_2O_7$ [M^{2+} = Mg (Calvo, 1965*a*, 1967; Lukaszewicz, 1967*a*), Cr (Glaum *et al.*, 1991; Gerk, 1996), Mn (Lukaszewicz & Smajkiewicz, 1961; Stefanidis & Nord, 1984), Fe (Baur & Tillmanns, 1986; Hoggins *et al.*, 1983), Co (Krishnamachari & Calvo, 1972; El Belghitti *et al.*, 1994; Forsyth *et al.*, 1989; El Bali & Bolte, 2002), Ni (Lukaszewicz, 1967*b*; Pietraszko & Lukaszewicz, 1968), Cu (Robertson & Calvo, 1967, 1968; Effenberger, 1990), Zn (Robertson & Calvo, 1970; Calvo, 1965*b*)] belong to the thortveitite structure family [*e.g.* $Sc_2Si_2O_7$ (Zachariasen, 1930; Cruickshank *et al.*, 1962; Foord *et al.*, 1993)]. In contrast to the disilicates the diphosphates, apart from $Mn_2P_2O_7$, show at least one phase transition upon cooling from the monoclinic thortveitite structure ($C2/m$, Z = 2, $a \sim 6.6$, $b \sim 8.6$, $c \sim 4.6$ Å, $\beta \sim 103°$) to low-symmetry modifications. These phase transitions are primarily driven by the dynamics of the diphosphate groups. Careful structure refinements have clearly shown that for diphosphates with the ideal thortveitite structure [*e.g.* $Mn_2P_2O_7$, powder data at room temperature (Stefanidis & Nord, 1984), β-$Cr_2P_2O_7$, single-crystal data at 453 K (Glaum, 1999)] a dynamic disorder of bent diphosphate groups is a

Table 1
Survey of modifications and phase-transition temperatures observed for diphosphates $M_2P_2O_7$ (M^{2+} = Mg, Cr, Mn, Fe, Co, Ni, Cu, Zn).

Metal(II)	$T(\alpha \leftrightarrow \beta)$ (K)†	Additional phase transitions
Mg	341[a]	No
Cr	364[b]	$\alpha_1 \leftrightarrow \alpha_2$ at T = 285 K, $\alpha_2 \leftrightarrow \alpha_3$ at T = 345 K[b] Magnetic ordering at T_N = 17 K[c]
Mn	No transition[d]	Magnetic ordering at T_N = 13 K[e,f]
Fe	365[b]	Magnetic ordering below T_N = 14 K[f]
Co	577[d]	Magnetic ordering at T_N = 11 K[g]
Ni	838[h]	Magnetic ordering below T_N = 5 K[i]
Cu	339–348[d]	Magnetic ordering below T_N = 23 K[f]
Zn	405–428[d]	No

References: (*a*) Calvo (1967); (*b*) Glaum (2005); (*c*) Glaum (1999); (*d*) Robertson & Calvo (1968); (*e*) Collins *et al.* (1971); (*f*) Gerk (1996); (*g*) Forsyth *et al.* (1989); (*h*) Pietraszko & Lukaszewicz (1968); (*i*) Glaum & Reehuis (1998). † $T(\alpha \leftrightarrow \beta)$ denotes

more reasonable structure description than the assumption of linear $P_2O_7^{4-}$ units. With respect to the d^4 (Jahn–Teller active) electronic configuration of the Cr^{2+} ions in $Cr_2P_2O_7$ the question arises how disorder of the diphosphate groups and Jahn–Teller effect combine to affect the dynamic behaviour of the whole structure. Interestingly, for copper(II) diphosphate, containing the Jahn–Teller-active Cu^{2+} ions, just one phase transition from the high-temperature phase to α-$Cu_2P_2O_7$, stable at ambient temperature, has been reported. Table 1 gives a survey of modifications and phase-transition temperatures observed for diphosphates $M_2P_2O_7$. The numbers of different modifications observed for diphosphates $M_2P_2O_7$ (M^{2+}: Mg, Cr–Zn) and their notation are somewhat confusing. Generally, it is accepted that the modification with ideal thortveitite structure (high-temperature phase) is denoted as the β phase. The low-symmetry modifications are denoted as the α phases. A problem arises when, as observed for $Cr_2P_2O_7$, several low-symmetry modifications exist. We suggest the following notation for $Cr_2P_2O_7$

$$\underset{\text{commensurate}}{\alpha_1} \overset{285\ \text{K}}{\longleftrightarrow} \underset{\text{incommensurate}}{\alpha_2} \overset{345\ \text{K}}{\longleftrightarrow} \underset{??}{\alpha_3} \overset{364\ \text{K}}{\longleftrightarrow} \beta . \quad (1)$$

Magnetic ordering is observed in the α phases of paramagnetic metal diphosphates at low temperatures. We suggest denoting these magnetically ordered phases using primes, *i.e.* α_1'-$Cr_2P_2O_7$ denotes the magnetically ordered α_1 phase of $Cr_2P_2O_7$.

Further confusion is caused by the existence of additional polymorphs of the diphosphates $M_2P_2O_7$ [M^{2+} = Co (Kobashi *et al.*, 1997), Ni (Masse *et al.*, 1979), Zn (Bataille *et al.*, 1998)] that do not belong to the thortveitite structure family. It is not yet settled for all cases which modifications are the thermodynamically stable ones.

2. Experimental

$Cr_2P_2O_7$ is obtained as single phase by the synproportionation of CrP and $CrPO_4$ [see (2)] in sealed, evacuated silica tubes [T = 1273 K, 24 h, 240 mg iodine as mineralizer, $V \sim 17$ cm^3 (Glaum *et al.*, 1986; Glaum & Gruehn, 1989)]. The reaction yields a microcrystalline, light-blue powder. The slight surplus of CrP [ratio $n(CrPO_4)$:$n(CrP)$ = 5.9 rather than 7.0 as necessary according to (2)] is dissolved in the gas phase and ensures reducing conditions in the ampoule.

$$7CrPO_4(s) + CrP(s) \rightarrow 4Cr_2P_2O_7(s) \quad (2)$$

The synthesis and subsequent crystal growth of chromium(II) diphosphate by chemical vapour-phase transport (Schäfer, 1964; Gruehn & Glaum, 2000) are achieved in a one-pot reaction. In a temperature gradient of 1323 → 1223 K using iodine as the transport agent, migration rates of up to 3 mg of $Cr_2P_2O_7$ per hour are observed. Crystals of $Cr_2P_2O_7$ grow on the wall of the silica tube in the sink region. They can be removed using dilute hydrofluoric acid. Despite containing divalent chromium, $Cr_2P_2O_7$ is stable against oxidation in air and even boiling nitric acid does not oxidize the diphosphate.

From the single crystals obtained by the method described above several individuals were mounted on glass fibres and tested for their quality. The X-ray diffraction pattern of a selected crystal was measured using the four-circle diffractometer Xcalibur (Oxford Diffraction) with kappa geometry equipped with a CCD-detector Sapphire 2 and a conventional X-ray tube. In order to precisely determine the intensities of the satellite reflections ω scans were used with a rather narrow step of 0.3° and a long exposure time of 60 s per frame. The data collection was planned so as to achieve a highly redundant data set (see Table 2).[1] The absorption correction based on a crystal shape was performed.

3. Structure solution and refinement

3.1. Incommensurate structure of α_2-$Cr_2P_2O_7$

Careful examination of the positions of the peaks extracted from the CCD images obtained at room temperature showed that in addition to the main reflections located on points of reciprocal lattice, the diffraction pattern also contained strong satellite reflections that could be indexed with four integers as $\mathbf{H} = h\mathbf{a}^* + k\mathbf{b}^* + l\mathbf{c}^* + m\mathbf{q}$ with $\mathbf{q} = (-0.361, 0, 0.471)$ and $m \neq 0$. As the components of the $\mathbf{q}$ vector are significantly different from any simple commensurate value, the structure can be considered to be incommensurately modulated.

The standard method for handling incommensurately modulated structures is to use the superspace approach (de Wolff *et al.*, 1981; Janssen *et al.*, 1992; van Smaalen, 1995). The monoclinic lattice symmetry and the observed reflection conditions ($hklm, h + k = 2n$) and ($hk0m, m = 2n$) lead to the superspace group $C2/m(\alpha, \beta, 0)0s$ (monoclinic c axis) or its non-centrosymmetric subgroup $Cm(\alpha, \beta, 0)s$. Structure refinements confirmed the centrosymmetric superspace group.

The structure was solved directly in superspace with the charge-flipping algorithm (Oszlányi & Sütő, 2004; Palatinus, 2004), using the program *BayMEM* (van Smaalen *et al.*, 2003).

[1] Supplementary data for this paper are available from the IUCr electronic archives (Reference: SN5033). Services for accessing these data are described at the back of the journal.

Table 2
Experimental details.

	Incommensurate	Commensurate
Crystal data		
Chemical formula	$Cr_2P_2O_7$	$Cr_2P_2O_7$
M_r	277.9	277.9
Cell setting, superspace group	Monoclinic, $C2/m(\alpha, 0, \gamma)0s$	Monoclinic, $C2/m(\alpha, 0, \gamma)0s$
Temperature (K)	298	140
t_0	–	0
q vector	(−0.361 (1), 0, 0.471 (1))	(−1/3, 0, 1/2)
a, b, c (Å)	7.0192, 8.4063, 4.6264	7.0464, 8.4073, 4.6394
β (°)	108.6111	108.708
V (Å^3)	258.71	260.32
Z	2	2
Radiation type	Mo $K\alpha$	Mo $K\alpha$
Wavelength (Å)	0.7090	0.7090
μ (mm^{-1})	4.799	4.769
Crystal form, colour	Irregular column, sky blue, transparent	Irregular column, sky blue, transparent
Crystal size (mm)	0.14 × 0.09 × 0.04	0.14 × 0.09 × 0.04
Data collection		
Diffractometer	Xcalibur, Oxford Diffraction	Xcalibur, Oxford Diffraction
Detector	CCD Sapphire 2	CCD Sapphire 2
Method of measurement	ω scans	ω scans
Scan width (°)	0.3	0.3
Absorption correction	Based on crystal shape	Based on crystal shape
$2\theta_{max}$ (°)	52.6	52.6
No. of independent reflections (all/obs)	2409/1433	1598/1466
No. of independent main reflections (all/obs)	283/278	283/280
No. of independent first-order sat. (all/obs)	495/455	497/479
No. of independent second-order sat. (all/obs)	569/421	571/503
No. of independent third-order sat. (all/obs)	495/183	247/204
No. of independent fourth-order sat. (all/obs)	567/96	–
Criterion for observed reflections	$I > 3\sigma(I)$	$I > 3\sigma(I)$
Redundancy	8.47	7.99
Range of h, k, l	$-9 \Rightarrow h \Rightarrow 9$ $-10 \Rightarrow k \Rightarrow 10$ $-7 \Rightarrow l \Rightarrow 7$ $-4 \Rightarrow m \Rightarrow 4$	$-9 \Rightarrow h \Rightarrow 9$ $-10 \Rightarrow k \Rightarrow 10$ $-7 \Rightarrow l \Rightarrow 7$ $-2 \Rightarrow m \Rightarrow 3$
Refinement		
Refinement on	F	F
Weighting scheme	Based on measured s.u.'s, $w = 1/[\sigma^2(F) + 0.0004F^2)$	Based on measured s.u.'s $w = 1/[\sigma^2(F) + 0.0004F^2)$
R_{obs}/wR_{all}		
All reflections	0.0227/0.0577	0.0205/0.0435
Main reflections	0.0165/0.0408	0.0169/0.0418
First-order satellites	0.0177/0.0308	0.0188/0.0359
Second-order satellites	0.0329/0.0498	0.0265/0.0438
Third-order satellites	0.0905/0.1823	0.0475/0.0746
Fourth-order satellites	0.1962/0.3688	–
Goodness-of-it (obs/all)	1.53/1.61	1.63/1.71
No. of parameters	179	105
Extinction correction	Isotropic type I (Becker & Coppens, 1974)	Isotropic type I (Becker & Coppens, 1974)
Extinction coefficient	0.059 (10)	0.039 (9)
Refinement software	*JANA*2000 (Petříček *et al.*, 2000)	*JANA*2000 (Petříček *et al.*, 2000)
Source of atomic scattering factors	*International Tables for X-ray Crystallography* (Vol. C)	*International Tables for X-ray Crystallography* (Vol. C)

Computer programs used: *CrysalisCCD* (Oxford Diffraction, 2004), *BayMEM* (van Smaalen *et al.*, 2003), *JANA*2000 (Petříček *et al.*, 2000), *DIAMOND* (Brandenburg *et al.*, 1999).

This method allows for the solution of a modulated structure directly in superspace, *i.e.* without first solving the average structure. The output of the structure solution by charge flipping is an approximate electron density in three-dimensional space (for periodic structures) or in superspace (for incommensurately modulated structures). The resulting superspace electron density – even though calculated without any symmetry constraints – revealed the superspace symmetry $C2/m(\alpha, \beta, 0)0s$. After averaging the electron density according to this superspace symmetry we obtained a very good estimate of both the basic positions of the atoms and their modulation functions (Figs. 1 and 2).

The basic structure of chromium(II) diphosphate is of the thortveitite ($Sc_2Si_2O_7$) structure type (Fig. 3). This structure can be considered as being built of honeycomb layers of $Cr^{II}O_3$, with a structure similar to that found in corundum. These layers are connected by diphosphate groups located above the vacant position in the dioctahedral layer. The structure contains one independent atom of chromium and phosphorus and three independent O atoms.

Analysis of the superspace density map obtained by charge flipping revealed that the modulation of the Cr and O3 atoms should be described by a sawtooth modulation function (Petříček *et al.*, 1990) of width 1 (Fig. 1). The O2 atom showed a discontinuity in the modulation function (Fig. 2). Such a discontinuity could be modeled by shifting the O2 atom from the special position on the m_y mirror plane and describing its modulation by a crenel function of width 0.5 (van der Lee *et al.*, 1994). The action of the mirror plane, which includes a shift of $\frac{1}{2}$ along the internal dimension, generates the complementary part of the atomic domain, so that the total occupation of the O2 atom is 1 for the whole interval of x_4 (Fig. 4). Atoms P and O1 were only moderately modulated and they have been described by a continuous harmonic modulation in the initial model. The slope of the saw-tooth functions was also estimated from the electron density obtained by charge flipping. The initial structure model assembled in this way was then refined in the *JANA*2000 program (Petříček *et al.*, 2000) and

smoothly converged to a stable solution. The structure model was further improved by adding the harmonic positional modulation to atoms described by the crenel and sawtooth functions. The anisotropic displacement parameters (ADP) of all the atoms were also found to be modulated. The combination of the harmonic positional modulation functions with discontinuous modulation functions defined only on a subinterval of x_4 values leads to serious correlations between parameters. Therefore, an orthogonalized set of modulation functions was used for the O2 atom (van der Lee *et al.*, 1994).

Fourier syntheses indicated that even the P atom exhibited a discontinuity in the modulation function that correlated with the discontinuity in the modulation of O2 and could be described by a crenel function in a similar way to O2 (Fig. 4). This model was confirmed by a significant drop in the R values upon introduction of this modulation combined with two harmonic waves of positional modulation. Again, orthogonalized modulation functions had to be used for the P atom.

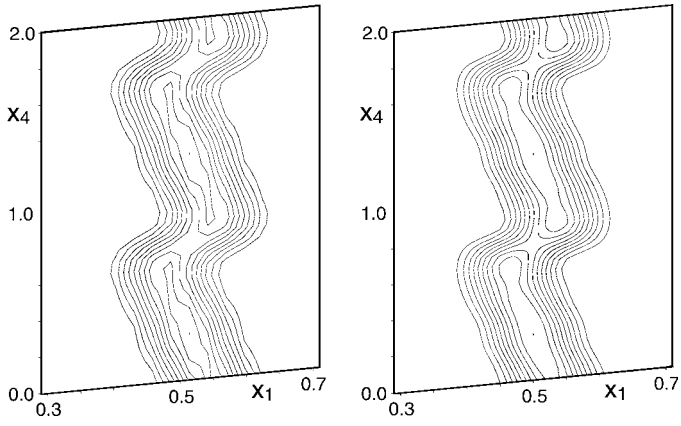

Figure 1
x_1–x_4 section through the superspace electron density at the position of the Cr atom. Left: as obtained from charge flipping. Right: as obtained from the final structure model. Contours at intervals of 10% of the maximum density.

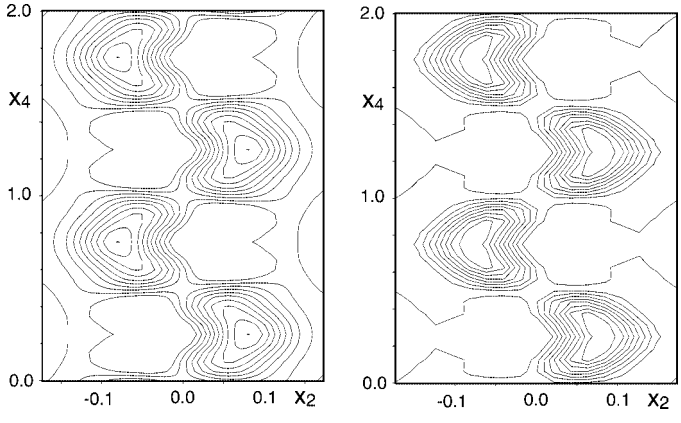

Figure 2
x_2–x_4 section through the superspace electron density at the position of the O2 atom. Left: as obtained from charge flipping. Right: as obtained from the final structure model. Contours at intervals of 10% of the maximum density.

As a next step the parameters of the special modulation functions (*i.e.* sawtooth and crenel functions) were considered. The centers of the special functions of atoms O2 and Cr are fixed by symmetry (twofold axis), while the centers of the special functions of atoms P and O3 are refinable in principle. However, to obtain a chemically reasonable model, the tightly bonded atoms (like those in the PO_4 tetrahedron) should have mutually correlated 'jumps' in the modulations. In other words, the discontinuities in the modulation functions of those atoms should occur at the same value of the internal coordinate t. This leads to the condition for the t values of the centers of the modulation functions: $t_{cen}(P) = t_{cen}(O2)$ and

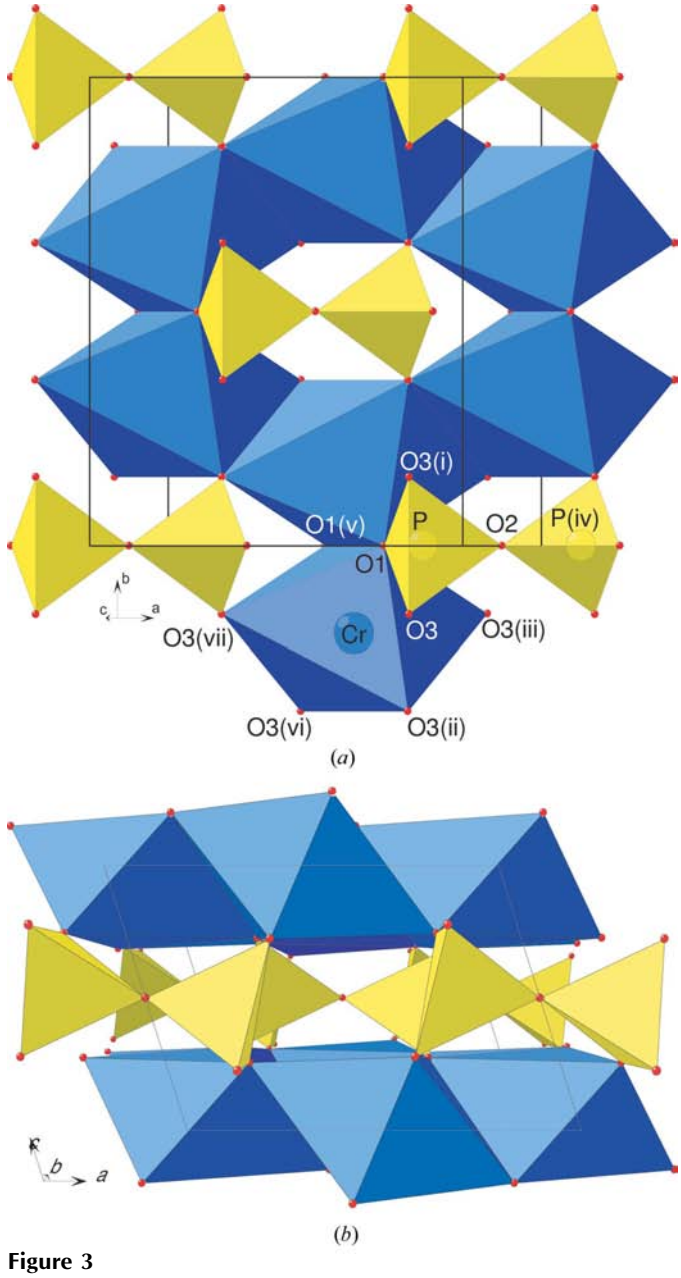

Figure 3
The basic structure of $Cr_2P_2O_7$ as viewed along **c*** (*a*) and **b** (*b*). Cr atoms are located at the centers of the distorted octahedra; P atoms lie in the centers of the tetrahedra. The labeled atoms correspond to the atoms listed in Table 5.

$t_{cen}(O3) = t_{cen}(O2) - 0.25$. Thus, because $t_{cen}(O2)$ is fixed by the symmetry, the centers of the special functions are fully determined by geometrical and chemical considerations and need not be refined. By analogy the definition intervals of the modulation functions of all the atoms (*i.e.* the interval along x_4 where the atom has a non-zero occupancy) are fixed by the requirement of a full occupancy of the atoms. A schematic representation of the modulation functions showing the mutual correlation of the discontinuities in the modulation functions in the PO_4 tetrahedron is shown in Fig. 4.

In the final stages of the refinement, only the modulation waves with significant components were retained, leading to four harmonic waves for the positional modulation of atoms Cr and O3, two positional modulation waves for atoms P, O1 and O2, and 4, 4, 2, 1, 0 modulation waves for the ADPs of atoms Cr, O3, O2, P and O1, respectively. The structure model just described will be denoted as Model *A* in the following.

There were several indications during the refinement process that Model *A* is not the best description of the structure. First, the difference Fourier map showed relatively high residual maxima up to 0.7 e $Å^{-3}$ at the positions of the Cr and O3 atoms. Second, the modulation of the displacement parameters required a large number of modulation waves to achieve reasonable lowering of the *R* values, and the ADPs at the vicinity of the discontinuities in the modulation functions were very large. Third, there was a shallow minimum in the plot of distance *versus* the internal coordinate *t* for the Cr and O3 atoms close to $t = 0.94$ (Fig. 5). This dent arose because of a slight misalignment of the discontinuities in the modulation functions of the Cr and O2, O3 atoms (Fig. 6). The Cr atom lies on a special position that fixes the discontinuity in its displacement modulation function to $x_4 = 0.75$. The position of the discontinuity of the O3 atom is fixed by the chemical considerations discussed above. That makes the slight misalignment in the modulation functions of Cr and O3 unavoidable. This problem can be overcome in the real structure by the disorder in the vicinity of the discontinuity in the modulation function. It seems reasonable that the local structure in the region close to the flip between two quite different configurations can randomly assume one or the other configuration. In order to model this behavior, we have shortened the full occupancy domains of the Cr, P, O2 and O3 atoms, and the emptied part of the x_4 interval was filled by half-occupied atoms. Counterparts of the half-occupied atoms were either added or generated by symmetry, thus creating disorder near the discontinuity. The principle of the improved model (Model *B*) is illustrated in Figs. 7 and 8. The width of the disordered domain refined to 0.084 (1). The introduction of the disorder led to a large improvement of the *R* values (Table 3). Moreover, after the introduction of the new atoms, many modulation waves of the ADPs of the main atoms became insignificant and could be removed. The total number of refinable parameters decreased from 200 in Model *A* to 179 in Model *B*, despite the introduction of six new atoms. The comparison of basic characteristics of the refinement for Model *A* and Model *B* is given in Table 3. It is reasonable to assume that the additional atoms may exhibit some positional and occupational modulation, which was however impossible

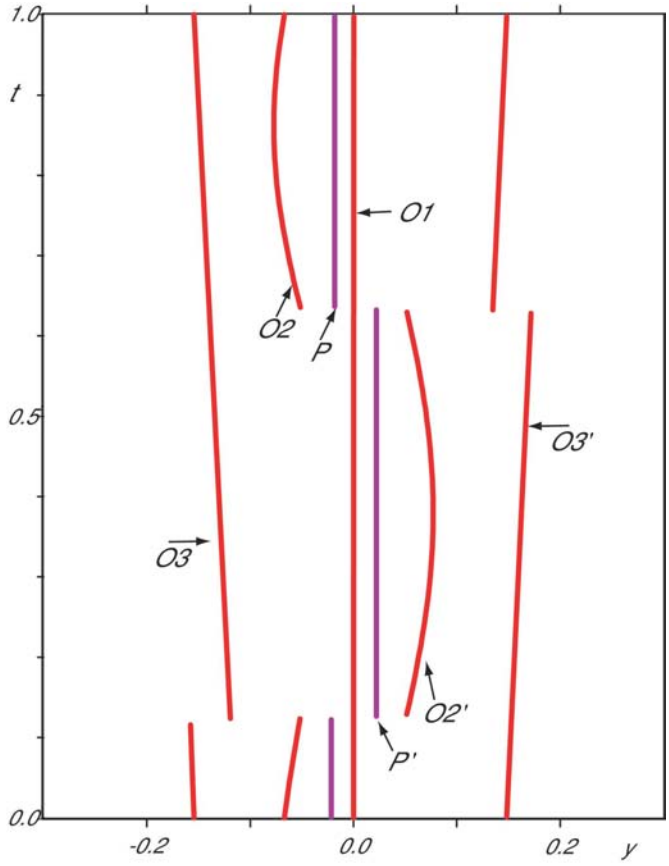

Figure 4
A scheme of the modulation functions of the atoms in the PO_4 group as a function of *t*. The *y* component of the modulation is shown. The modulation functions have been simplified to emphasize the basic trends. Each jump of the tetrahedron at the discontinuity can be understood as a rotation around an axis going through the O1 and one of the O3 atoms. Symmetry code: (i) $x_1, -x_2, x_3, \frac{1}{2} + x_4$.

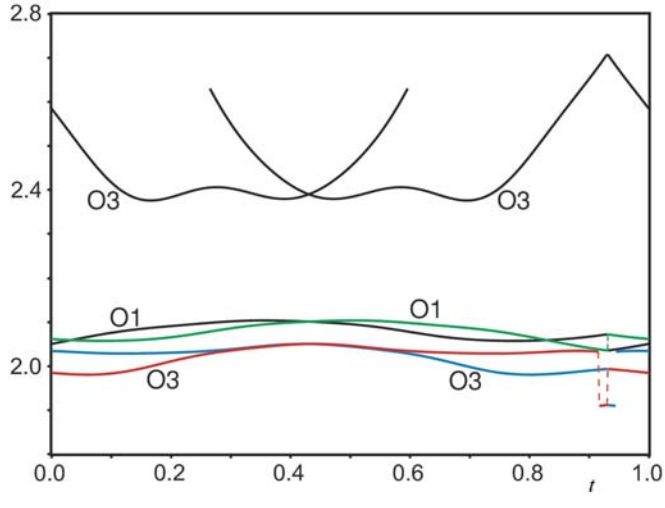

Figure 5
Distances Cr—O as a function of *t* in Model *A*. The dashed vertical lines connect parts of the discontinuous modulation curves Cr—O3 and Cr—O1. Note the dent in the modulation curve Cr—O3 around $t = 0.94$.

Table 3
Characteristics of model *A* and model *B* of the incommensurate structure of α_2-$Cr_2P_2O_7$.

	Model *A*	Model *B*
R values *R*(obs)/*wR*(all)		
All reflections	0.0299/0.0613	0.0227/0.0577
Main reflections	0.0214/0.0444	0.0165/0.0408
First-order satellites	0.0275/0.0382	0.0177/0.0308
Second-order satellites	0.0440/0.0596	0.0330/0.0498
Third-order satellites	0.1020/0.1863	0.0906/0.1822
Fourth-order satellites	0.1840/0.3431	0.1962/0.3688
No. of parameters	200	179
Positional/ADP harmonic modulation waves		
Cr	4/4	4/2
P	2/1	2/1
O1	3/0	2/0
O2	2/3	1/0
O3	4/4	3/1

to refine due to the very small width of the occupational domain of these atoms. Owing to this limitation the modulation curves and the interatomic distances are not smooth through the transition between the main atom and its disordered counterpart. Moreover, the presence of two disordered positions makes the curves look very complicated. Therefore, for the sake of simplicity and legibility we omit the disordered regions from Figs. 9, 10 and 11.

3.2. Commensurate structure of α_1-$Cr_2P_2O_7$

$Cr_2P_2O_7$ undergoes a lock-in phase transition into a commensurately modulated structure with $\mathbf{q} = (-\frac{1}{3}, 0, \frac{1}{2})$ at T_c = 285 K. The diffracted intensities were measured at T = 140 K. It is one of the advantages of the superspace description of modulated structures that the phases related by a lock-in phase transition can be described using the same basic unit cell and superspace symmetry. Therefore, the structure model of the incommensurate phase could be used as a starting model for the refinement of the commensurate phase. For commensurate refinement one has to choose the value of t_0 that determines which superspace symmetry operation will be realised in the three-dimensional supercell. In the present case, the combination of the superspace group

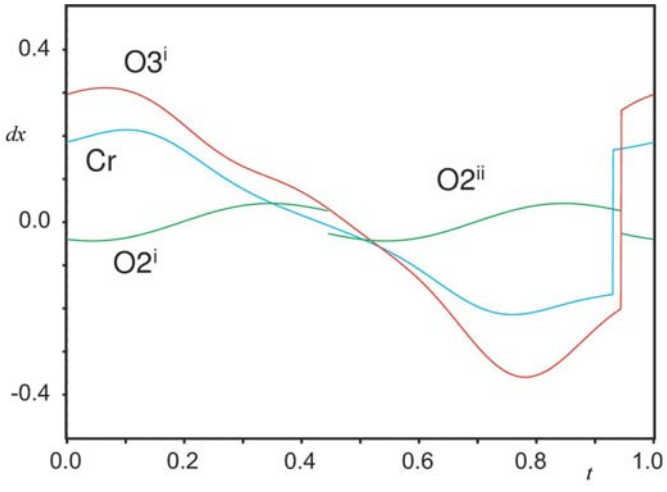

Figure 6
Displacements along *x* of the Cr, O2 and O3 atoms as a function of *t*. The discontinuities in the modulation of O2 and O3 occur at the same $t = 0.944$, but the discontinuity of the Cr atom (t = 0.930) is slightly shifted. The two discontinuities in the curve for O2 are symmetrically related. Symmetry codes: (i) $\frac{3}{2} - x_1$, $-\frac{1}{2} - x_2$, $1 - x_3$, $-x_4$; (ii) $\frac{3}{2} - x_1$, $-\frac{1}{2} + x_2$, $1 - x_3$, $\frac{1}{2} - x_4$.

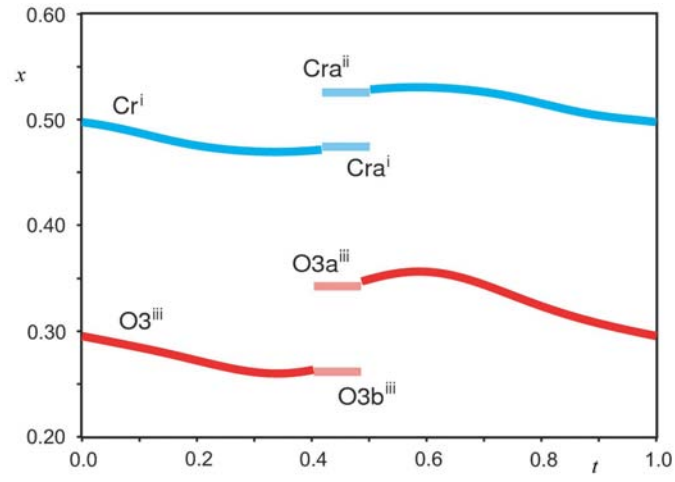

Figure 7
The *x* coordinate of the Cr and O3 atoms as a function of *t* in model *B*. Straight lines in lighter colors indicate the half-occupied additional atoms designed so that their occupational domains overlap. Symmetry codes: (i) $x_1, x_2, 1 + x_3, x_4$; (ii) $1 - x_1, x_2, 1 - x_3, \frac{1}{2} - x_4$; (iii) $-\frac{1}{2} + x_1, -\frac{1}{2} - x_2, x_3, \frac{1}{2} + x_4$. For the sake of clarity the symmetry codes were selected so that the disordered region is located in the middle of the plot.

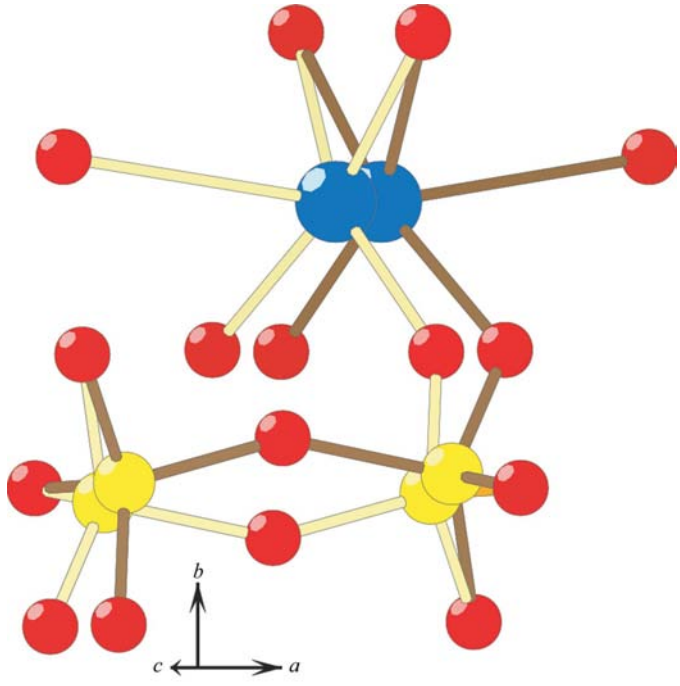

Figure 8
Scheme of the disordered structure (model *B*) close to the point of discontinuity in the modulation functions. The disordered structure assumes two configurations represented by the light and dark bonds between atoms.

Table 4
No. of modulation waves in the superspace description of the lock-in phase of α_1-$Cr_2P_2O_7$.

Fractional numbers (*e.g.* 2.5) mean that from the parameters of the last wave only half are independent (for instance, the sine terms) and thus only half of the wave can be used. In the case of O3 and Cr atoms, the half-wave of the positional modulation is represented by the parameters of the saw-tooth function.

	Maximum allowed number of modulation waves	Significant waves in the final model (positional/ADP)
Cr	2.5	2.5/1
P	1	1/0
O1	2.5	2.5/0
O2	1	1/0
O3	2.5	2.5/2

$C2/m(\alpha, 0, \gamma)0s$ with $\mathbf{q} = (-\frac{1}{3}, 0, \frac{1}{2})$ leads to two possible space-group symmetries of the sixfold superstructure: $I2/c$ for $t_0 = n/12, n = 0,...,11$ and Ic for the alternative values of t_0. Our refinement confirmed the centrosymmetric space group $I2/c$.

Owing to the commensurability of the low-temperature structure, only a limited number of modulation waves can be refined. Parameters of redundant modulation waves would be totally correlated. Although the restrictions on the number and type of the modulation waves can be derived directly from the superspace formalism, a much more convenient way from the practical point of view is to use the comparison with the structure expanded into the sixfold supercell. The number of independent parameters of any atom in the modulated description (basic position + all modulation waves) must not exceed the number of corresponding refinable parameters of all atoms in the supercell derived from this atom. Using this procedure, the limits on the number of allowed modulation waves were established as listed in Table 4.

It should be noted that no special modulation functions are necessary in the commensurate refinement, since the limited number of the atomic positions can always be described by a finite number of harmonic modulation waves. However, in the present case the special modulation functions were retained to allow for an easy comparison of the modulation functions of the commensurate and incommensurate structure.

Commensurate refinement using the maximum number of refinable parameters (151 parameters) converged to an R value of 0.019. Inspection of the refined parameters showed that many of the modulation waves for ADPs were insignificant. These insignificant waves were eliminated, leading to only 105 refinable parameters and the final R value of 0.021. The final numbers of modulation waves are listed in Table 4.

In Figs. 9 and 10 the Cr—O and P—O distances plotted as a function of t are compared with those of the incommensurate phase. For the commensurate phase only six isolated configurations are realised for $t = n/6$, n = 0,...,5, and only corresponding distances can be found in the sixfold superstructure. These six values of t do not intersect the intervals with disorder in the incommensurate structure. For this reason Model *B* and all related discussions about the position of the discontinuities are irrelevant for the commensurate case.

The commensurate structure can be described and refined in a sixfold supercell $a' = 3a$, $b' = b$, $c' = 2c$ and $\beta' = \beta$ with the symmetry $I2/c$. The symmetry of the commensurate structure is a subgroup of the order 6 of the basic structure symmetry, but due to the special positions of some atoms only three, three, three, two and six non-equivalent atoms are generated from atoms Cr, P, O1, O2 and O3 of the basic structure, respectively. It has been already mentioned that the sixfold supercell and the commensurate description have the same number of refinable parameters, namely 151, because both models are just alternative descriptions of the same structure. The R values (R_{obs}) of the refinement are the same

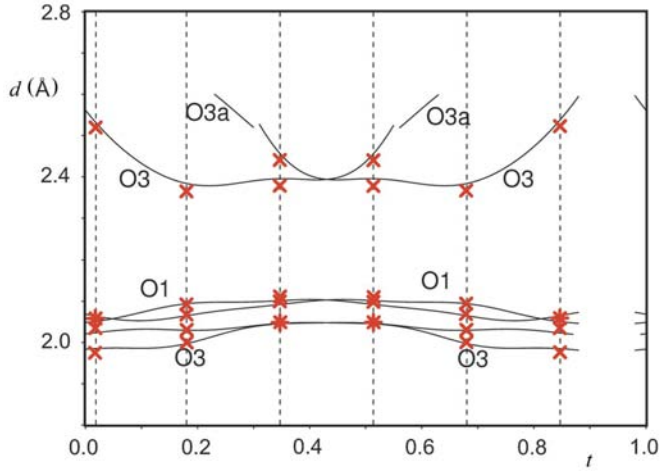

Figure 9
Cr—O distances as a function of the internal coordinate t. Lines show the distances in the incommensurate structure and crosses mark the distances in the commensurate structure at the six realised sections (indicated by the dashed vertical lines). The disordered part of the incommensurate structure is omitted. Stars are used instead of crosses at four places, where the crosses of two independent atoms would be indistinguishably close.

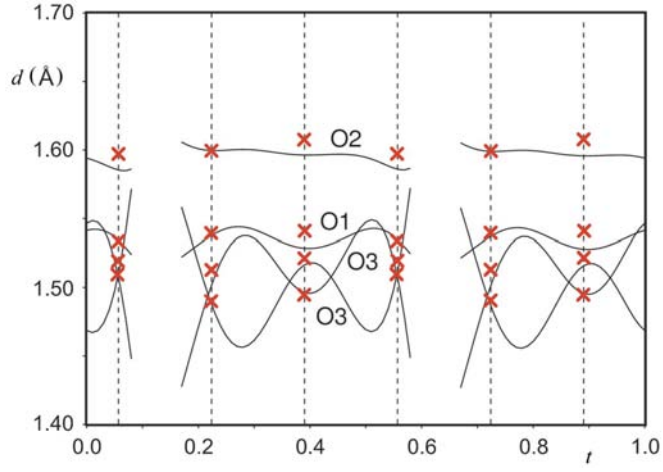

Figure 10
P—O distances as a function of the internal coordinate t. Lines show the distances in the incommensurate structure and crosses mark the distances in the commensurate structure at the six realised sections (indicated by the dashed vertical lines). The disordered part of the incommensurate structure is omitted.

for the two descriptions for the same reason. The resulting structure is thus the same whether refined in the supercell or in superspace, if the full number of refinable parameters is used.[2]

The superspace description provides a convenient and efficient means of reducing the number of refinement parameters. It separates the average structure from the deviation of each group of atoms from the average. In this way it is easy to recognize that certain parameters do not significantly vary between the atoms in the supercell and do not need to be refined. In the present case, the number of parameters was reduced by 30% with only a marginal increase of the refinement R values. On the contrary, no such separation is possible in the supercell description, where each independent atom has its own set of structure parameters.

Other arguments for the use of the superspace approach for the description of commensurate structures are as follows:

(i) Parameters of atoms that are independent in the supercell are often heavily correlated. The possibility of eliminating the insignificant modulation parameters can prevent this type of correlation and often leads to a more stable refinement.

(ii) The partial R values for the satellites provide a sensitive measure of the quality of the fit to the superstructure features.

(iii) The superspace structure model is directly related to the model of the incommensurate counterpart. This facilitates the comparison between the structures. It is also possible to use the structure model of one structure as a starting model for the structure solution of the other structure.

(iv) A unified structure description is possible for a whole family of related structures (see §4).

For these reasons we use the superspace description of the commensurate phase α_1-$Cr_2P_2O_7$ throughout this paper. The refinement details for both structures are summarized in Table 2 and the structure parameters for both structures (for the commensurate structure in both the superspace and supercell descriptions) have been deposited.

4. Discussion

4.1. The origin of the modulation

The basic structure of $Cr_2P_2O_7$ is of the thortveitite type with the general composition $M_2A_2O_7$. The structure is formed by sheets of distorted MO_6 octahedra with one third of the octahedral positions unoccupied. These vacant octahedral positions are bridged from each side of the layer by an A_2O_7 group (compare the basic structure of $Cr_2P_2O_7$ in Fig. 3). The symmetry of the structure requires that the two A atoms and the bridging oxygen of the A_2O_7 group have on average a linear configuration. However, the P_2O_7 groups adopt a bent configuration, which is favored over the linear configuration by considerations of chemical bonding. In the high-temperature, thermally activated structure this mismatch between the symmetry of the P_2O_7 group and the global symmetry leads to a dynamic disorder of P_2O_7 (Stefanidis & Nord, 1984; Glaum, 1999). Upon lowering the temperature, the presence of low-symmetrical (bent) diphosphate groups in a rather high-symmetrical void leads to a phase transition towards a structure with lower symmetry. A similar mechanism applies to the other members of the family of metal diphosphates (Table 1).

However, this mechanism alone cannot explain the incommensurability of the structure at room temperature and an additional distortion is needed, whose interaction with the main distortion mode would lead to the incommensuration of the structure. Although we were not able to directly identify this secondary distortion, one possibility is that this distortion could be due to the Jahn–Teller activity of the Cr^{2+} ion. This proposition can explain the presence of only one structural phase transition in most other metal diphosphates studied so far (Table 1), because these structures do not contain Jahn–Teller active ions. The only other known structure of this family containing a Jahn–Teller active ion is $Cu_2P_2O_7$, reported to have only one phase transition (Robertson & Calvo, 1967). However, the α and β phases of $Cu_2P_2O_7$ coexist in a wide temperature range of more than 30 K and the phase transition is accompanied by structured diffuse scattering. Thus, a possibility of structural instability between the α and β phases and the influence of the Jahn–Teller activity of the Cu^{2+} ion cannot be excluded. Thermal as well as structural studies to clarify this point are currently being carried out at our laboratories.

What remains unknown up to now is the role of the α_3 phase of $Cr_2P_2O_7$ that has been observed in the DSC measurement. Its structure has not yet been determined and is currently being studied.

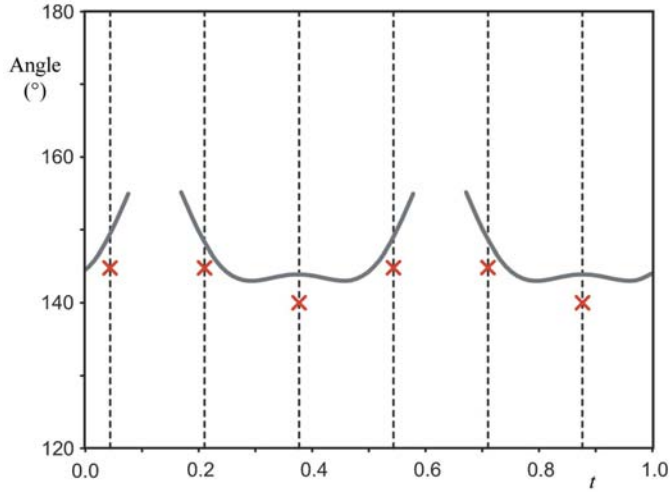

Figure 11
P—O2—P angle as a function of the internal coordinate t. Lines show the distances in the incommensurate structure and crosses mark the distances in the commensurate structure at the six realised sections (indicated by the dashed vertical lines). Note that the two parts of the curve correspond to two alternating orientations of the P_2O_7 groups with the acute P—O—P angle pointing towards +**b** and −**b**, respectively (see Fig. 12). The disordered part of the incommensurate structure is omitted.

[2] Occasionally small differences between the two refinements can occur due to numerical reasons.

Table 5
Selected distances (Å) and angles (°) in the incommensurate and commensurate structure.

	Incommensurate			Commensurate		
	Ave.	Min.	Max.	Ave.	Min.	Max.
P—O1	1.53 (4)	1.52 (3)	1.54 (5)	1.538 (2)	1.534 (2)	1.541 (2)
P—O2	1.60 (6)	1.59 (7)	1.61 (5)	1.601 (2)	1.597 (2)	1.608 (2)
P—O3	1.51 (7)	1.43 (5)	1.55 (8)	1.518 (4)	1.513 (3)	1.521 (4)
P—O3^{i}	1.49 (8)	1.46 (10)	1.57 (8)	1.498 (4)	1.490 (4)	1.509 (3)
Cr—O1	2.079 (2)	2.046 (2)	2.104 (3)	2.081 (2)	2.059 (2)	2.109 (2)
Cr—O3^{ii}	2.023 (4)	1.981 (4)	2.048 (4)	2.023 (4)	1.977 (4)	2.049 (3)
Cr—O3^{iii}†	2.710 (4)	2.378 (5)	3.431 (5)	2.769 (5)	2.366 (3)	3.487 (6)
Cr—O3^{ii} ‡	2.428 (4)	2.378 (5)	2.597 (5)	2.426 (4)	2.366 (3)	2.526 (4)
Cr—O3^{ii} §	3.363 (5)	3.239 (5)	3.431 (5)	3.454 (5)	3.421 (5)	3.486 (6)
O1—P—O2	105 (2)	101 (2)	109 (3)	105.4 (1)	103.4 (1)	107.1 (1)
O1—P—O3	112 (4)	110 (5)	117 (3)	111.4 (2)	111.0 (2)	111.9 (2)
O1—P—O3^{i}	111 (5)	108 (5)	113 (6)	111.1 (2)	110.4 (1)	111.8 (2)
O2—P—O3	103 (4)	101 (5)	109 (3)	103.5 (2)	102.2 (2)	105.4 (2)
O2—P—O3^{i}	111 (4)	106 (4)	113 (4)	111.0 (2)	110.5 (2)	111.5 (2)
O3—P—O3^{i}	114 (3)	113 (2)	115 (3)	113.9 (2)	113.4 (2)	114.4 (2)
P—O2—P^{iv}	146 (4)	143 (4)	155 (3)	143.3 (3)	140.1 (4)	144.9 (2)
O1—Cr—O1^{v}	79.93 (9)	78.94 (8)	81.67 (9)	80.26 (6)	79.13 (6)	81.90 (7)
O1—Cr—O3^{ii}	95.19 (11)	92.75 (11)	97.00 (11)	94.95 (10)	92.88 (13)	96.55 (10)
O1—Cr—O3^{vi}	165.17 (15)	160.22 (15)	169.20 (15)	166.28 (14)	161.13 (14)	170.14 (16)
O1^{v}—Cr—O3^{ii}	165.23 (15)	160.22 (15)	169.21 (15)	166.28 (14)	161.13 (14)	170.15 (16)
O1—Cr—O3^{iii}	83.86 (11)	76.40 (9)	89.29 (11)	83.15 (9)	75.35 (8)	90.43 (8)
O3^{ii}—Cr—O3^{iii}	80.28 (15)	78.50 (15)	84.22 (14)	81.00 (15)	78.87 (18)	84.60 (17)
O3^{vi}—Cr—O3^{iii}	110.00 (15)	106.52 (16)	112.07 (14)	109.39 (15)	106.60 (17)	112.14 (19)
O1—Cr—O3^{vii}	85.76 (11)	79.29 (9)	91.00 (11)	85.76 (9)	78.71 (9)	92.54 (9)
O1^{v}—Cr—O3^{vii}	83.72 (11)	76.39 (9)	89.29 (11)	83.15 (9)	75.35 (8)	90.43 (8)
O3^{ii}—Cr—O3^{vii}	110.06 (15)	106.52 (16)	112.07 (14)	109.39 (15)	106.60 (17)	112.14 (19)
O3^{vi}—Cr—O3^{vii}	80.34 (15)	78.50 (15)	84.22 (14)	80.99 (15)	78.86 (18)	84.60 (17)
O3^{iii}—Cr—O3^{vii}	165.32 (14)	163.83 (13)	166.7 (2)	165.37 (10)	164.11 (8)	166.56 (14)

Symmetry codes: (i) $x_1, -x_2, x_3, \frac{1}{2}+x_4$; (ii) $\frac{3}{2}-x_1, -\frac{1}{2}-x_2, 1-x_3, -x_4$; (iii) $x_1, x_2, -1+x_3, x_4$; (iv) $2-x_1, x_2, 1-x_3, \frac{1}{2}-x_4$; (v) $1-x_1, -x_2, -x_3, -x_4$; (vi) $-\frac{1}{2}+x_1, -\frac{1}{2}-x_2, -1+x_3, \frac{1}{2}+x_4$; (vii) $1-x_1, x_2, 1-x_3, \frac{1}{2}-x_4$. † Distance of chromium to the apical oxygen over the full *t* range (including distances in both the coordinated and non-coordinated configurations). ‡ Distance of chromium to the apical oxygen in the *t* range where the apical oxygen closely coordinates chromium (compare Fig. 9). § Distance of chromium to the apical oxygen in the *t* range where the apical oxygen does not coordinate chromium.

4.2. The incommensurately modulated structure

The principal consequence of the modulation is a formation of clusters of Cr coordination polyhedra, consisting typically of one central CrO_6 octahedron with two adjacent CrO_5 square pyramids. This regular pattern is occasionally disturbed by an irregularity resulting from the incommensurability of the structure. The sequence of the polyhedra along **a** can be schematically noted as 5-6-5 5-6-5 with the occasional occurrence of a 5-6-5-5 motif. In this notation the number represents the coordination number of the central atom, the dash connects two edge-sharing polyhedra and space separates two neighboring polyhedra that do not share any atom (compare Fig. 12). The formation of clusters is realised through bending of the P_2O_7 group at O2 and rotation of the PO_4 tetrahedra accompanied by large shifts of the Cr atoms mostly along **a**. As a result of the clustering the coordination polyhedra of Cr become more regular than in the average structure. The longest Cr—O distance decreases by 0.2–0.4 Å from 2.74 Å in the average structure to a value typically between 2.38 and 2.60 Å in the modulated structure (Fig. 9). The distances between the central Cr atom and the equatorial O atoms are almost unaffected by the modulation, suggesting that their distance is close to the chemical optimum.

Table 5 contains a summary of selected distances and angles in the structure. Inspection of this table shows that the changes in the distance of chromium to the apical oxygen is indeed the main consequence of the modulation. While this distance varies dramatically in a range that exceeds 1 Å, all other distances are stable typically within the interval of 0.1 Å.

4.3. The commensurate structure

The overall picture of the commensurate structure is very similar to its incommensurate counterpart. However, instead of an infinite number of possible *t*-sections in the incommensurate structure, only six sections are realised (Fig. 9). The six- and fivefold coordinated Cr atoms form a regular sequence of one octahedron with two adjacent square pyramids along **a**, denoted schematically as 5-6-5 5-6-5 (see Fig. 12).

The models of the incommensurate and commensurate structures are best compared by means of the comparison of distances and angles (Figs. 9, 10 and 11, Table 5). These plots and the table show that the structure model of

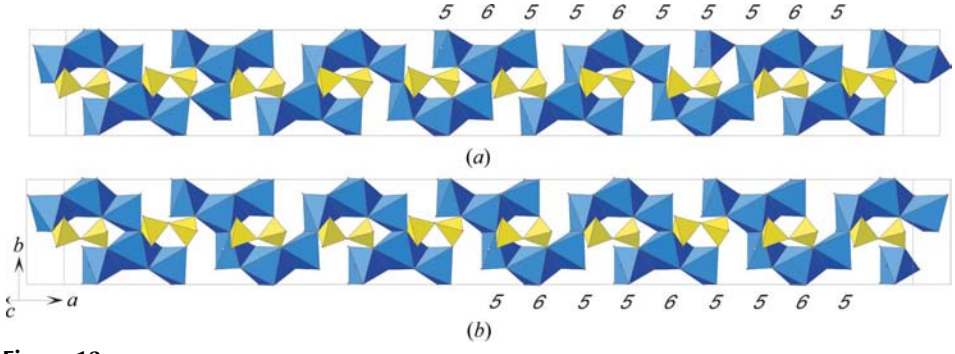

Figure 12
Two rows of the coordination polyhedra of Cr (blue) and the attached P_2O_7 groups (yellow) viewed along **c***. Ten unit cells of the basic structure are shown along **a** and one unit cell along **b** and **c**. (*a*) Incommensurate structure; (*b*) commensurate structure. The sequence of the coordination numbers of the Cr atoms is indicated. The irregularities in the 5-6-5 5-6-5 pattern are visible at two places of the incommensurate structure.

Table 6
Survey of the symmetries of the low-temperature phases of diphosphates $M_2P_2O_7$ (M^{2+} = Mg, Cr, Co, Ni, Cu, Zn).

The parent superspace group of the structures is $C2/m(\alpha, 0, \gamma)0s$. The symmetry of the supercell can be derived from this superspace group using the tabulated **q** vector and t_0.

	q vector	t_0	Space group of the supercell
Cr, Zn	$(-\frac{1}{3}, 0, \frac{1}{2})$	0	$I2/c$
Co, Mg, Ni	$(\frac{1}{2}, 0, \frac{1}{2})$	$\frac{1}{8}$	$B2_1/c$
Cu	$(0, 0, \frac{1}{2})$	0	$C2/c$

the incommensurate structure fits the commensurate structure very well, with differences in the distances of the order of a few hundredths of Å. Moreover, these differences can probably be ascribed to the fact that the two structures were determined at two quite different temperatures (Table 2). The slight decrease of the angles P—O2—P by about 4° between the incommensurate and commensurate phases is also probably a result of the lowering of the thermal motion upon cooling, because all distances and angles are uncorrected for thermal motion.

It is interesting to compare the commensurate structure of α_1-$Cr_2P_2O_7$ with the low-temperature α-phases of other transition metal diphosphates. A survey of the crystal structures available at the inorganic crystal structure database (ICSD) reveals that out of seven structures with transition metals between Cr and Cu, the Mn member has no phase transition, for the Fe member the low-temperature structure is not known with sufficient accuracy, and the others (Cr, Co, Ni, Zn, Cu) have structures very similar to that of the α phase. Their symmetries can be derived from the same superspace group using various **q**-vectors (Table 6). The same description is also valid for the structure of α-$Mg_2P_2O_7$. The difference in the structures is mainly in the variation of the coordination polyhedra along **a**. The overall scheme denoted as 5-6-5 (Fig. 12) is valid for the Cr member and the isostructural Zn member, while the Cu member exhibits a 5-5 scheme and the Mg, Ni and Co members of the series exhibit a 5-6-6-5 ordering.

5. Conclusions

Chromium(II) diphosphate in its α_2 phase has an incommensurately modulated structure at room temperature with $\mathbf{q} = (-0.361, 0, 0.471)$. This structure transforms into a commensurate α_1 phase with $\mathbf{q} = (-\frac{1}{3}, 0, \frac{1}{2})$ at $T = 285$ K. The incommensurate–commensurate phase transition is a typical lock-in phase transition. Both structures can be described in superspace with the same superspace group $C2/m(\alpha, 0, \gamma)0s$ and with very similar structure models.

Chromium(II) diphosphate is exceptional among the metal diphosphates in that it exhibits three phase transitions, while at most one phase transition is observed for the other diphosphates. We suggest that this complex behavior is due to the Jahn–Teller activity of the Cr^{2+} ion. The incommensurability of the room-temperature structure would then be a result of the competition between the structural distortions due to the dynamics of the P_2O_7 group and due to the Jahn–Teller distortion of the coordination of the Cr^{2+} ion. An interesting prospect is to investigate the details of the phase transition of the copper(II) diphosphate, another diphosphate with a Jahn–Teller active ion, and look for the demonstration of the Jahn–Teller activity of the Cu^{2+} ion in analogy to what is observed in chromium(II) diphosphate.

The superspace structural model of the α_2-phase can be considered a parent model for the whole family of the low-temperature structures of metal diphosphates (Table 6). Structures of the five known members of this family can all be described by one superspace structural model. Individual structures are obtained by the variation of the **q** vector and t_0. This family is an example of a group of structures that are related by the same superspace symmetry and can be described by one general structure model in superspace. An example of such a unified description that has been extensively discussed in the literature are the compositionally flexible perovskite-related compounds (Elcoro *et al.*, 2000, 2001, 2003; Perez-Mato *et al.*, 1999; Evain *et al.*, 1998; Gourdon *et al.*, 2000; Darriet *et al.*, 2002). Another example is a group of A_2BX_4 compounds (Chen & Walker, 1990). The unified description of structural families with a superspace structure model offers possibilities such as structure prediction, building structure models for new structures from known structures of other members of the family, or finding structural relations and underlying physical phenomena among structures with different unit-cell dimensions and space groups, but with similar basic structure and superspace group.

We would like to express our thanks to Dr Václav Petříček for fruitful discussions and suggestions for improvements. We also thank Mgr Karla Fejfarová for her assistance with the experimental part of the work. This work was supported by the Grant Agency of the Czech Republic, grant No. 202/03/0430.

References

Bataille, W. H., Benard-Rocherulle, P. & Louer, D. (1998). *J. Solid State Chem.* **140**, 62–70.
Baur, W. H. & Tillmanns, E. (1986). *Acta Cryst.* B**42**, 95–111.
Becker, P. J. & Coppens, P. (1974). *Acta Cryst.* A**30**, 129–152.
Brandenburg, K. (1999). *DIAMOND*, Version 2.1c. Crystal Impact GbR, Bonn, Germany.
Calvo, C. (1965*a*). *Can. J. Chem.* **43**, 1139–1146.
Calvo, C. (1965*b*). *Can. J. Chem.* **43**, 1147–1153.
Calvo, C. (1967). *Acta Cryst.* **23**, 289–295.
Chen, Z. Y. & Walker, M. B. (1990). *Phys. Rev. B*, **43**, 5634–5648.
Collins, M. F., Gill, G. S. & Stager, C. V. (1971). *Can. J. Phys.* **49**, 979–982.
Cruickshank, D. W. J., Lynton, H. & Barclay, G. A. (1962). *Acta Cryst.* **15**, 491–498.
Darriet, J., Elcoro, L., El Abed, A. & Perez-Mato, J. M. (2002). *Chem. Mater.* **14**, 3349–3363.
Effenberger, H. (1990). *Acta Cryst.* C**46**, 691–692.
El Bali, B. & Bolte, M. (2002). *Acta Cryst.* E**58**, i32–i33.
El Belghitti, A., Boukhari, A. & Holt, E. M. (1994). *Acta Cryst.* C**50**, 482–484.

Elcoro, L., Perez-Mato, J. M., Darriet, J. & El Abed, A. (2003). *Acta Cryst.* B**59**, 217–233.
Elcoro, L., Perez-Mato, J. M. & Withers, R. (2000). *Z. Kristallogr.* **215**, 717–739.
Elcoro, L., Perez-Mato, J. M. & Withers, R. (2001). *Acta Cryst.* B**57**, 471–484.
Evain, M., Boucher, F., Gourdon, O., Petříček, V., Dušek, M. & Bezdička, P. (1998). *Chem. Mater.* **10**, 3068–3076.
Foord, E., Birmingham, S. D., Demartin, F., Pilati, T., Gramaccioli, C. M. & Lichte, F. (1993). *Can. Miner.* **31**, 337–346.
Forsyth, J. B., Wilkinson, C., Paster, S. & Wanklyn, B. M. (1989). *J. Phys. Condens. Matter*, **1**, 169–178.
Gerk, M. (1996). PhD Thesis. University of Gießen, Germany.
Glaum, R. (1999). Thesis of Habilitation (in German). University of Gießen, Germany; http://bibd.uni-giessen.de/ghtm/1999/uni/h990001.htm.
Glaum, R. (2005). Unpublished results. University of Bonn.
Glaum, R. & Gruehn, R. (1989). *Z. Anorg. Allg. Chem.* **573**, 24–42.
Glaum, R., Gruehn, R. & Möller, M. H. (1986). *Z. Anorg. Allg. Chem.* **543**, 111–116.
Glaum, R. & Reehuis, M. (1998). Unpublished results. Hahn–Meitner Institute, Berlin.
Glaum, R., Walter-Peter, M., Özalp, D. & Gruehn, R. (1991). *Z. Anorg. Allg. Chem.* **601**, 145–162.
Gourdon, O., Petříček, V. & Evain, M. (2000). *Acta Cryst.* B**56**, 409–418.
Gruehn, R. & Glaum, R. (2000). *Angew. Chem. Int. Ed.* **39**, 692–716.
Hoggins, J. T., Swinnea, J. S. & Steinfink, H. (1983). *J. Solid State Chem.* **47**, 278–283.
Janssen, T., Janner, A., Looijenga-Vos, A. & de Wolff, P. M. (1992). *International Tables for Crystallography*, Vol. C, edited by A. J. C. Wilson, p. 797. Dordrecht: Kluwer Academic Publishers.
Kobashi, D., Kohara, S., Yamakawa, J. & Kawahara, A. (1997). *Acta Cryst.* C**53**, 1523–1525.
Krishnamachari, N. & Calvo, C. (1972). *Acta Cryst.* B**28**, 2883–2885.
Lee, A. van der, Evain, M., Monconduit, L., Brec, L., Rouxel, J. & Petříček, V. (1994). *Acta Cryst.* B**50**, 119–128.
Lukaszewicz, K. (1967*a*). *Bull. Acad. Pol. Sci. Ser. Sci. Chim.* **15**, 53–57.
Lukaszewicz, K. (1967*b*). *Bull. Acad. Pol. Sci. Ser. Sci. Chim.* **15**, 47–51.
Lukaszewicz, K. & Smajkiewicz, R. (1961). *Rocz. Chem.* **35**, 741–744.
Masse, R., Guitel, J. C. & Durif, A. (1979). *Mater. Res. Bull.* **14**, 337–341.
Oszlányi, G. & Sütő, A. (2004). *Acta Cryst.* A**60**, 134–141.
Oxford Diffraction (2004). *Crysalis CCD*, CCD Data Collection GUI. Oxford Diffraction Ltd, Oxford, UK.
Palatinus, L. (2004). *Acta Cryst.* A**60**, 604–610.
Perez-Mato, J. M., Zakhour-Nakhl, M., Weill, F. & Darriet, J. (1999). *J. Mater. Chem.* **9**, 2795–2808.
Petříček, V., Dušek, M. & Palatinus, L. (2000). *JANA*2000. Institute of Physics, Praha, Czech Republic.
Petříček, V., Gao, Y., Lee, P. & Coppens, P. (1990). *Phys. Rev. B*, **42**, 387–392.
Pietraszko, A. & Lukaszewicz, K. (1968). *Bull. Acad. Pol. Sci. Ser. Sci. Chim.* **16**, 183–187.
Robertson, B. E. & Calvo, C. (1967). *Acta Cryst.* **22**, 665–672.
Robertson, B. E. & Calvo, C. (1968). *Can. J. Chem.* **46**, 605–612.
Robertson, B. E. & Calvo, C. (1970). *J. Solid State Chem.* **1**, 120–133.
Schäfer, H. (1964). *Chemical Transport Reactions.* New York: Academic Press.
Smaalen, S. van (1995). *Crystallogr. Rev.* **4**, 79–202.
Smaalen, S. van, Palatinus, L. & Schneider, M. (2003). *Acta Cryst.* A**59**, 459–469.
Stefanidis, T. & Nord, A. G. (1984). *Acta Cryst.* C**40**, 1995–1999.
Wolff, P. M. de, Janssen, T. & Janner, A. (1981). *Acta Cryst.* A**37**, 625–636.
Zachariasen, W. H. (1930). *Z. Kristallogr.* **73**, 1–6.